



**Providing Choice & Value**

Generic CT and MRI Contrast Agents



CONTACT REP

**AJNR**









This information is current as  
of July 19, 2025.

**Callosal Interhemispheric Communication in  
Mild Traumatic Brain Injury: A Mediation  
Analysis on WM Microstructure Effects**

Sohae Chung, Tamar Bacon, Joseph F. Rath, Alaleh Alivar,  
Santiago Coelho, Prin Amorapanth, Els Fieremans, Dmitry  
S. Novikov, Steven R. Flanagan, Joshua H. Bacon and  
Yvonne W. Lui

*AJNR Am J Neuroradiol* published online 18 April 2024  
<http://www.ajnr.org/content/early/2024/04/18/ajnr.A8213>

# Callosal Interhemispheric Communication in Mild Traumatic Brain Injury: A Mediation Analysis on WM Microstructure Effects

 Sohae Chung,  Tamar Bacon,  Joseph F. Rath,  Alaleh Alivar,  Santiago Coelho,  Prin Amorapanth,  Els Fieremans,  Dmitry S. Novikov,  Steven R. Flanagan, Joshua H. Bacon, and  Yvonne W. Lui



## ABSTRACT

**BACKGROUND AND PURPOSE:** Because the corpus callosum connects the left and right hemispheres and a variety of WM bundles across the brain in complex ways, damage to the neighboring WM microstructure may specifically disrupt interhemispheric communication through the corpus callosum following mild traumatic brain injury. Here we use a mediation framework to investigate how callosal interhemispheric communication is affected by WM microstructure in mild traumatic brain injury.

**MATERIALS AND METHODS:** Multishell diffusion MR imaging was performed on 23 patients with mild traumatic brain injury within 1 month of injury and 17 healthy controls, deriving 11 diffusion metrics, including DTI, diffusional kurtosis imaging, and compartment-specific standard model parameters. Interhemispheric processing speed was assessed using the interhemispheric speed of processing task (IHSPT) by measuring the latency between word presentation to the 2 hemivisual fields and oral word articulation. Mediation analysis was performed to assess the indirect effect of neighboring WM microstructures on the relationship between the corpus callosum and IHSPT performance. In addition, we conducted a univariate correlation analysis to investigate the direct association between callosal microstructures and IHSPT performance as well as a multivariate regression analysis to jointly evaluate both callosal and neighboring WM microstructures in association with IHSPT scores for each group.

**RESULTS:** Several significant mediators in the relationships between callosal microstructure and IHSPT performance were found in healthy controls. However, patients with mild traumatic brain injury appeared to lose such normal associations when microstructural changes occurred compared with healthy controls.

**CONCLUSIONS:** This study investigates the effects of neighboring WM microstructure on callosal interhemispheric communication in healthy controls and patients with mild traumatic brain injury, highlighting that neighboring noncallosal WM microstructures are involved in callosal interhemispheric communication and information transfer. Further longitudinal studies may provide insight into the temporal dynamics of interhemispheric recovery following mild traumatic brain injury.

**ABBREVIATIONS:** aCR/sCR/pCR = anterior/superior/posterior corona radiata; aIC/pIC/rIC = anterior/posterior/retrolenticular limb of the internal capsule; CC = corpus callosum; Cg = cingulum (cingulate gyrus); Ch = cingulum (hippocampus);  $D_a$  = intra-axonal diffusivity;  $D_e^{\parallel}$  = extra-axonal axial diffusivity;  $D_e^{\perp}$  = extra-axonal radial diffusivity; DKI = diffusional kurtosis imaging;  $f$  = axonal water fraction; FA = fractional anisotropy; gCC/bCC/sCC = genu/body/splenium of corpus callosum; IHSPT = interhemispheric speed of processing task; L = left; LVF = left visual field; MD/AD/RD = mean/axial/radial diffusivities; MK/AK/RK = mean/axial/radial kurtosis; MTBI = mild traumatic brain injury; R = right; RT = reaction time; RVF = right visual field; SFOF = superior fronto-occipital fasciculus; SLF = superior longitudinal fasciculus; SM = standard model; TBSS = Tract-Based Spatial Statistics

Mild traumatic brain injury (MTBI), commonly known as concussion, is a major public health problem with potentially

serious clinical sequelae for weeks to months after injury or even longer.<sup>1,2</sup> It is known that stretch and torsion injury to the WM can occur after head injury and that the corpus callosum (CC) is particularly at risk.<sup>3,4</sup> Several MTBI studies using diffusion MR imaging to study human brain microstructure corroborate findings from biomechanical modeling reflective of this finding.<sup>5-8</sup>

The CC forms a critical central pathway for interhemispheric communication and information transfer. Damage to the CC is likely to impact normal interhemispheric communication<sup>9,10</sup> and could contribute to the complex and subtle symptoms central to MTBI.<sup>11,12</sup> Indeed, some prior studies have shown that callosal degradation may influence the information transfer and integration

Received May 26, 2023; accepted after revision January 27, 2024.

From the Department of Radiology (S. Chung, A.A., S. Coelho, E.F., D.S.N., Y.W.L.), Center for Advanced Imaging Innovation and Research, Department of Radiology (S. Chung, A.A., S. Coelho, E.F., D.S.N., Y.W.L.), Bernard and Irene Schwartz Center for Biomedical Imaging, and Departments of Neurology (T.B., J.H.B.), and Rehabilitation Medicine (J.F.R., P.A., S.R.F.), New York University Grossman School of Medicine, New York, New York.

This work was supported by the National Institutes of Health R01 NS119767-01A1, R01 NS039135-11, R56 NS119767, P41 EB017183, and the Department of Defense PT190013.

Please address correspondence to Sohae Chung, PhD, 660 1st Ave, 4th floor, New York, NY 10016; e-mail: sohae.chung@nyulangone.org

 Indicates article with online supplemental data.

<http://dx.doi.org/10.3174/ajnr.A8213>

between the hemispheres in patients with CC degradation as well as in normal aging.<sup>13</sup> Also, an association between posterior callosal atrophy and slowed cross-hemisphere processing of visual information has been shown in patients with MS.<sup>14</sup> However, impairments relating to callosal injury are not easily identified. Further complicating the situation, the CC does not function alone but instead connects adjacent WM bundles across the brain in an intricate way<sup>15</sup> that could mediate the callosal interhemispheric communication.

Because MTBI comprises a heterogeneous group of injuries and manifests as a heterogeneous group of symptoms, there is a great need for focused studies of region-specific injury and its impact on specific functional domains. Therefore, the purpose of this work is to study how callosal interhemispheric communication is affected by WM microstructure in patients with MTBI compared with healthy controls. Callosal and neighboring WM microstructures are studied in both healthy controls and patients with MTBI using advanced diffusion MR imaging methods

including DTI,<sup>16</sup> diffusional kurtosis imaging (DKI),<sup>17</sup> and the standard model (SM) of diffusion in WM<sup>18,19</sup> to tap tissue microstructure noninvasively. While DTI and DKI parameters are, by design, not specific to tissue components,<sup>20</sup> the SM can estimate biophysically more meaningful and compartment-specific parameters of tissue microstructure,<sup>21,22</sup> including axonal water fraction ( $f$ ), intra-axonal diffusivity ( $D_a$ ), and extra-axonal axial and radial diffusivities ( $D_e^||$  and  $D_e^\perp$ , respectively). Several studies including animal validation<sup>21,23</sup> and in vivo human studies<sup>6,24-27</sup> suggest that these parameters are more informative than empirical diffusion measures.

A visual stimulus-response test, the interhemispheric speed of processing task (IHSPT),<sup>14</sup> has been used in this work to assess interhemispheric processing speed. The IHSPT measures latency in articulating a word presented to the left hemi-visual field, requiring information to travel across hemispheres (Fig 1). It has been shown that performance on this task is facilitated through the CC, a critical pathway for interhemispheric communication.<sup>14,28</sup> Here, we hypothesize that there are measurable changes in neighboring WM microstructures in patients with MTBI that may disrupt the callosal interhemispheric communication. A mediation framework is used to investigate how a neighboring WM microstructure (ie, mediator) indirectly affects the association between callosal microstructure and interhemispheric processing in MTBI (Fig 2B). In addition, a univariate correlation analysis is performed to investigate the direct association between callosal microstructures and IHSPT performance, and a multivariate regression analysis is performed to jointly evaluate both callosal and neighboring WM microstructures simultaneously in association with IHSPT performance for each group.

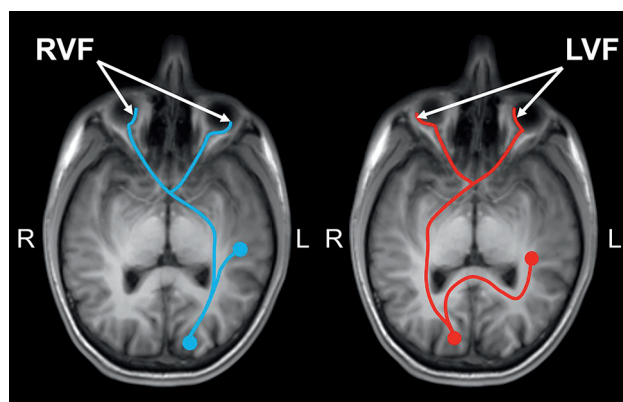


**FIG 1.** A schematic illustration of the IHSPT probes of hemispheric and callosal WM integrity by measuring processing speed and latency in the articulation of words presented to the LVF and RVF in individuals with left-hemisphere language dominance and vice versa for right-hemisphere-dominant individuals. For individuals with left-language dominance (most), visual information presented to the RVF projects to the left primary visual cortex with access to primary language centers in the same hemisphere (blue), whereas visual information from the subject's LVF projects to the contralateral (right) primary visual cortex and must then cross the midline to access core language centers in the left brain (red). A difference in latency between presentation and oral articulation of the word can be measured to tap interhemispheric processing speed.

## MATERIALS AND METHODS

### Study Population

This study has been approved by our Institutional Review Board, and all experiments were performed under relevant guidelines and regulations. All subjects were prospectively recruited from the Institutional Concussion Center or Emergency Department and provided written informed consent before the procedure. Inclusion criteria were the following: 1) age range of 18–65 years, 2) diagnostic MTBI criteria defined by the American Congress of Rehabilitation Medicine<sup>29</sup> including loss of consciousness of <30 minutes, and 3) brain injury within 1 month. We excluded patients with the following: 1) a reported history of head trauma, neurologic illness, or psychiatric disorders; 2) a history of participation in organized contact sports; 3) any contraindication to MR imaging; and 4) non-right-handed individuals to avoid the confounding effects of handedness in IHSPT test performance.

We studied 23 patients with MTBI (mean age, 36 [SD, 14] years; 9 men) and 17 healthy controls (mean age, 34 [SD, 1] years; 8 men). Postconcussion symptoms were assessed by using the Rivermead Postconcussion Symptoms Questionnaire.<sup>30</sup> The mean total scores of this questionnaire for patients with

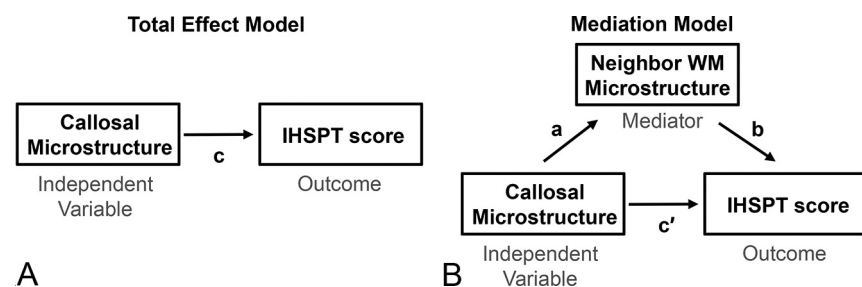


**FIG 2.** Path diagrams illustrate the total (or entire) effect model (A) and the mediation model (B).<sup>19</sup> The mediation model decomposes the total effect,  $c$ , into the direct effect,  $c'$ , and the indirect effect,  $ab = c - c'$ , where  $a$  is the independent-mediator effect and  $b$  is the mediator-outcome effect. The paths  $a$ ,  $b$ ,  $c$ , and  $c'$  represent the regression coefficients.

## Characteristics of the patients and healthy controls

	Patients with MTBI (n = 23)	Healthy Controls (n = 17)
Male/female	9:14	8:9
Age (mean) (yr)	36 (SD, 14)	34 (SD, 11)
Education (mean) (yr)	16 (SD, 2)	17 (SD, 2)
Time since injury (mean) (days)	18 (SD, 8)	—
Injury mechanism (No.)		
Hit by object	8	
Fall	8	
Car collision	4	
Assault	1	
Other	2	
RPQ total score (mean)	23 (SD, 16)	6 (SD, 8)
IHSPT score (mean) (range) (%)	5.8 (SD, 5.7) (0.1–25.6)	5.2 (SD, 3.1) (0.3–10.8)

**Note:**—RPQ indicates Rivermead Postconcussion Symptoms Questionnaire; IHSPT; Interhemispheric Processing Speed Test.

MTBI were 23 (SD, 16). The characteristics of the study population are summarized in the Table. For all subjects, brain MR imaging and an IHSPT test were acquired within 1 week of each other.

### MR Imaging Acquisition

MR imaging was performed on 3T MR imaging scanners (Magnetom Skyra or Magnetom Prisma, Siemens), with 23 subjects using Magnetom Skyra and 17 using Magnetom Prisma. Multishell diffusion imaging was performed with 5 b-values (250, 1000, 1500, 2000, 2500 s/mm<sup>2</sup>) along with 5 diffusion-encoding direction schemes (6, 20, 20, 30, 60, respectively) using multiband (factor of 2)<sup>31</sup> EPI for accelerated acquisitions with an anterior-posterior phase-encoding direction. Other parameters included the following: FOV = 220 × 220 mm, matrix = 88 × 88, number of slices = 56, 2.5-mm isotropic resolution, a partial Fourier factor = 6/8, TR/TE = 4900/95 ms, bandwidth = 2104 Hz/pixel, a generalized autocalibrating partially parallel acquisition factor of 2. Three nonweighted diffusion images (b = 0 s/mm<sup>2</sup>) were also acquired. An additional image with b = 0 s/mm<sup>2</sup> with a reversed phase-encoding direction was acquired for geometric artifact correction.<sup>32</sup>

### IHSPT

The IHSPT test was used to evaluate the interhemispheric speed of processing by measuring latency between words presented to the left visual field (LVF) and right visual field (RVF) and the subject's oral articulation of these words.<sup>14</sup> This test links visual perception and expressive language, specifically testing interhemispheric communication between primary visual and language pathways. For left-language-dominant individuals, words presented to the RVF project to the left hemisphere, and the average reaction time (RT) between presentation and articulation (Fig 1, blue) is slightly faster than for words presented to the LVF, which project to the right hemisphere and then are required to cross the midline to access core language centers in the left hemisphere (Fig 1, red). This process is reversed for right-language-dominant individuals. The test was performed using E-Prime 2.0 software (Psychology Software Tools) to control the precision of visual stimulus presentation and data collection. Each trial consisted of a simple 3-letter word randomly presented for 150 ms to either the LVF or RVF. Subjects were instructed to speak the word as quickly as possible, and the RT between presentation

and articulation was recorded automatically. Eighty random trials were conducted from a set of 110 three-letter words. Trials were excluded if the RT was 2 SDs above or below the subject's own mean (considered distraction or a possible unrelated vocal trigger). The IHSPT test score (percentage) was calculated using the absolute difference of the median RTs for LVF and RVF word presentations, divided by the average RT between them, and then multiplied by 100 to obtain a percentage score. Note that to account for individual variabilities

of language dominance, the absolute difference of the RTs was used.

### Image Analyses

**Diffusion Image Processing.** Denoising for the DWIs was performed using the Marchenko-Pastur principal component analysis method.<sup>33</sup> By means of the Diffusion parameter Estimation with Gibbs Noise removal (DESIGNER) pipeline (<https://github.com/NYU-DiffusionMRI/DESIGNER-v2>),<sup>34</sup> denoised diffusion images were corrected for Gibbs ringing artifacts<sup>35</sup> and then were rigidly aligned and corrected for eddy current distortions and subject motion simultaneously.<sup>36</sup> EPI-included distortions were also corrected using a b = 0 image with reverse phase-encoding.<sup>32</sup> For DTI parameters, a b-value of 1000 was used. In total, 11 diffusion metrics including DTI (fractional anisotropy [FA], mean/axial/radial diffusivities [MD/AD/RD]), DKI (mean/axial/radial kurtosis [MK/AK/RK]), and SM metrics ( $f$ ,  $D_a$ ,  $D_e^||$ ,  $D_e^\perp$ ) were calculated using in-house software (SMI toolbox; <https://www.smisupplychain.com/tools/smi-toolbox/>).<sup>19,37</sup> To minimize scanner variability, we used ComBat (<https://github.com/Jfortin1/ComBatHarmonization>)<sup>38,39</sup> for harmonization of diffusion parametric maps, preserving biologic variabilities such as age, sex, and disease group.

**Tract-Based Spatial Statistics.** Voxelwise group comparisons of diffusion metrics were performed using Tract-Based Spatial Statistics (TBSS)<sup>36</sup> with age as a covariate. Briefly, all subjects' FA maps were projected to the FA skeleton template (Montreal Neurological Institute 152 space), which was thresholded at an FA of 0.3 to restrict the analysis to WM regions with highly aligned fiber bundles. Other diffusion maps underwent unified processes by projecting them to the FA skeleton. Voxelwise analysis was then performed on the skeleton for each diffusion parameter.

**ROI.** Twenty-seven ROIs were explored on the basis of being major cerebral WM tracts, including the genu, body, splenium of the CC (gCC, bCC, sCC), right and left anterior, posterior, retrolenticular limb of the internal capsule (aIC, pIC, rIC), anterior, superior, posterior corona radiata (aCR, sCR, pCR), posterior thalamic radiation, external capsule, cingulum (cingulate gyrus) (Cg), cingulum (hippocampus) (Ch), superior longitudinal fasciculus (SLF), and superior fronto-occipital fasciculus (SFOF), respectively. ROIs were generated on the basis of the John Hopkins

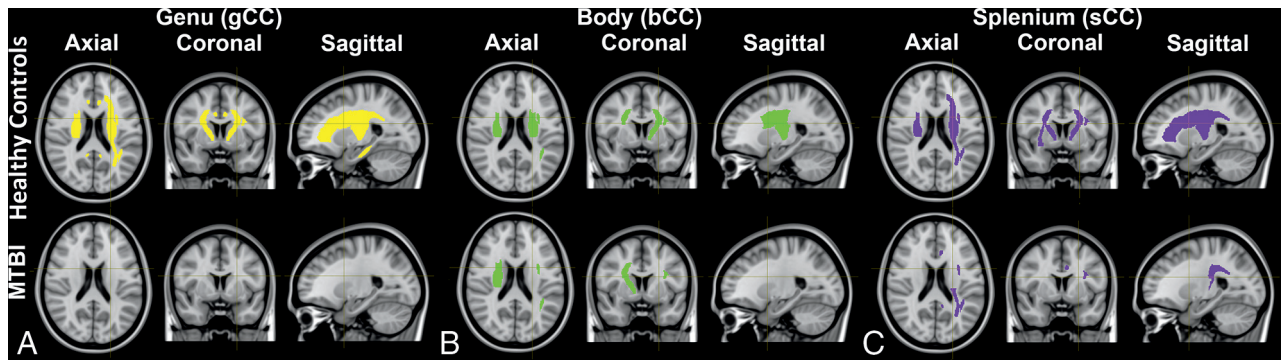


**FIG 3.** Mediation analysis demonstrates significant indirect mediators (neighbor WM ROIs) in the relationships (A) between the genu of the CC and IHSPT performance including areas (yellow) of aIC, pIC, rIC, aCR<sub>L</sub>, sCR, pCR<sub>L</sub>, Cg, Ch<sub>L</sub>, SLF<sub>L</sub>, and SFOF in healthy controls (*upper row*) and no area in patients with MTBI (*lower row*); (B) between the body of the CC and IHSPT performance including areas (green) of aIC<sub>L</sub>, pIC, rIC<sub>R</sub>, sCR, SLF<sub>L</sub>, and SFOF<sub>L</sub> in healthy controls (*upper row*) and aIC<sub>R</sub>, sCR<sub>R</sub>, SLF<sub>L</sub>, and SFOF<sub>R</sub> in patients with MTBI (*lower row*); and (C) between the splenium of the CC and IHSPT performance including areas (purple) of aIC, pIC, rIC<sub>R</sub>, aCR<sub>L</sub>, sCR, pCR<sub>L</sub>, EC<sub>R</sub>, Ch<sub>R</sub>, SLF<sub>L</sub>, and SFOF<sub>L</sub> in healthy controls (*upper row*) and rIC<sub>L</sub>, pCR<sub>L</sub>, Cg<sub>L</sub>, and SLF<sub>L</sub> in patients with MTBI (*lower row*). Details are in the Online Supplemental Data.

University ICBM-DTI-81 WM Atlas labels<sup>40</sup> by nonlinearly registering each subject's FA map to the FA template using FSL (<http://www.fmrib.ox.ac.uk/fsl>).<sup>36</sup> A reversed warping procedure was performed to assign the atlas labels to each subject's space. All ROIs were manually reviewed and edited as needed. For each ROI, the mean value of each diffusion metric was obtained only in voxels with FA  $\geq 0.3$  to restrict the analysis to WM regions.

### Statistical Analyses

Groups were compared in terms of sex using a Fisher exact test and in terms of age using an exact Mann-Whitney *U* test. Group differences on the IHSPT scores were assessed with 1-way ANCOVA with age as a covariate.

Mediation analysis was performed to decompose the total effect of the CC microstructure on IHSPT (*c* in Fig 2A) into a direct effect (*c'* in Fig 2B) and an indirect, mediated effect (*ab* in Fig 2B) through 1 mediator (ie, neighbor WM microstructure), where the paths *a*, *b*, *c'*, and *c* represented the regression coefficients in Fig 2. The mediation model used in this work included 1 mediator as shown in Fig 2B. Mediation analysis was conducted using PROCESS<sup>41</sup> in the SPSS (SPSS) framework with 5000 bootstrap resamples adjusted for age. A significant mediated effect was determined if the 95% CI did not contain zero.

In addition, we conducted a univariate correlation analysis with age as a covariate to investigate the association between callosal microstructures and IHSPT performance as well as a multivariate regression analysis to jointly evaluate both callosal and neighboring WM microstructures in association with IHSPT scores for each group. We used SPSS, Version 28.

For TBSS, statistical analysis was conducted with 5000 random permutations to identify statistically significant voxels, corrected for multiple comparisons with threshold-free cluster enhancement. For ROI analysis, MANCOVA, was performed by adjusting for age. The level of significance was set at  $P < .05$ .

### RESULTS

Groups were not significantly different in terms of sex ( $P = .75$ , Fisher exact test), age ( $P = .98$ , Mann-Whitney *U* test), and IHSPT scores ( $P = .65$ , ANCOVA).

Mediation analysis found several significant mediators in the healthy control group, located mostly in an array of areas: 1) between gCC and IHSPT: aIC, pIC, rIC, aCR<sub>L</sub>, sCR, pCR<sub>L</sub>, Cg<sub>R</sub>, Ch<sub>L</sub>, SLF<sub>L</sub>, SFOF; 2) between bCC and IHSPT: aIC<sub>L</sub>, pIC, rIC<sub>R</sub>, sCR, SFOF<sub>L</sub>; and 3) between sCC and IHSPT: aIC, pIC, rIC<sub>R</sub>, sCR<sub>L</sub>, EC<sub>R</sub>, Ch<sub>R</sub>, SFOF<sub>L</sub> (Fig 3, *upper row*). Patients with MTBI appeared to lose some of the normal associations (Fig 3, *lower row*). More details are summarized in the Online Supplemental Data.

Significant univariate correlations and a trend toward significance between the CC and IHSPT scores were observed in the healthy control group: gCC ( $D_a$ ,  $r = 0.51$ ,  $P = .046$ ;  $D_e^||$ ,  $r = -0.49$ ,  $P = .052$ ) and sCC ( $D_a$ ,  $r = 0.46$ ,  $P = .071$ ;  $D_e^||$ ,  $r = -0.58$ ,  $P = .019$ ), but these relationships were not seen in the MTBI group. Multivariate regression analysis also found significant associations of several WM regions with IHSPT scores mainly including gCC, sCC, aIC<sub>L</sub>, pIC<sub>R</sub>, rIC<sub>R</sub>, sCR<sub>L</sub>, SFOF<sub>L</sub> in the healthy control group, but fewer WM regions in the MTBI group (Online Supplemental Data), showing consistent results with the results of mediation analysis.

Group differences were revealed using TBSS analysis in several diffusion maps (Fig 4). There were significantly different areas demonstrating lower FA, MK, AK, RK in the MTBI group compared with the healthy control group as well as areas demonstrating higher MD, AD, RD,  $D_a$ , and  $D_e^+$  in MTBI, mainly in left-sided WM regions including bCC, aIC<sub>L</sub>, aIC<sub>L</sub>, aCR<sub>L</sub>, sCR<sub>L</sub>, pCR<sub>L</sub>, EC<sub>L</sub>, Cg<sub>L</sub>, SLF<sub>L</sub> and SFOF<sub>L</sub>. The results of ROI analyses were consistent with TBSS results (Online Supplemental Data).

### DISCUSSION

In this study, univariate analysis has found significant correlations between callosal microstructures and IHSPT performance in the healthy control group because we know that the callosum serves as a link between 2 cerebral hemispheres, allowing them to communicate. However, these relationships have not been seen in the MTBI group. Moreover, we have found several significant mediators in the healthy control group, involving mainly bilateral WM regions including capsular WM, the corona radiata, cingulum,

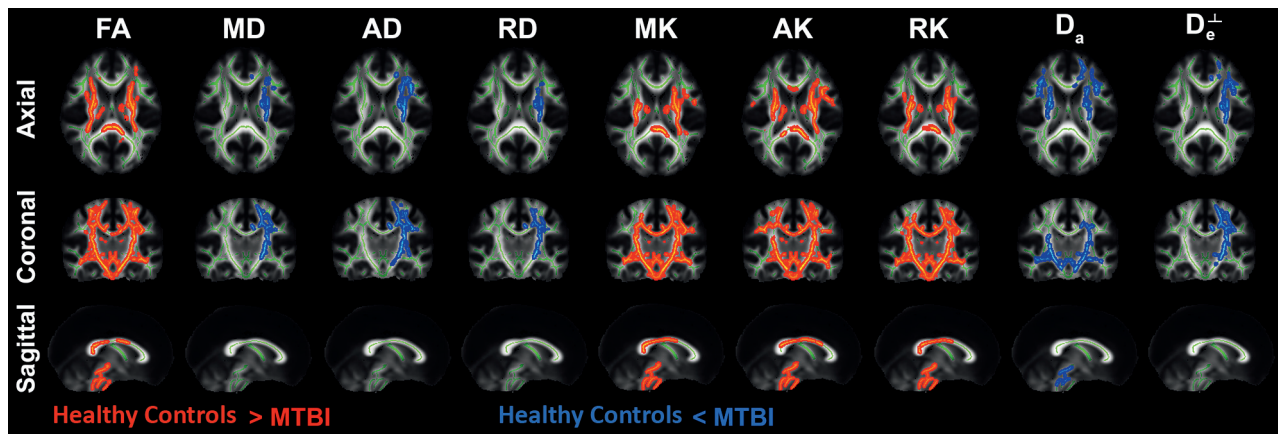


**FIG 4.** TBSS results comparing diffusion measures between MTBI and healthy control groups. Clusters of voxels (red) demonstrating significantly lower FA, MK, AK, and RK in the MTBI group compared with the healthy control group ( $P < .05$ , family-wise error-corrected) are present diffusely across the entire WM. Increased MD, AD, RD,  $D_a$ , and  $D_e^\perp$  are seen in mainly left-sided, WM regions including bCC, aCL, pCL, aCR<sub>L</sub>, sCR<sub>L</sub>, pCR<sub>L</sub>, EC<sub>L</sub>, Cg<sub>L</sub>, SLF<sub>L</sub>, and SFOF<sub>L</sub> in the MTBI group. A heat map showing differences between groups is overlaid on the mean FA template and WM skeleton (green).

SLF, and SFOF (Fig 3, upper row). These results support the idea that callosal interhemispheric communication is also mediated by neighboring WM microstructures. This mediation is plausible because we know that the CC is not an isolated structure. However, in patients with MTBI, we found a loss of normal mediators, suggesting the anticipated disruption of normal relationships possibly due to increased IHSPT scores (ie, slowing of interhemispheric communication) that may be related to microstructural changes after injury (Fig 3, lower row). Our finding is supported by the TBSS results showing microstructural alterations in patients with MTBI compared with healthy controls (Fig 4), in keeping with prior diffusion findings indicative of extra-axonal changes such as vasogenic edema in the acute and subacute periods of injury considered reversible.<sup>42</sup> In particular, extra-axonal diffusion markers,  $D_e^\parallel$  and  $D_e^\perp$ , have been suggested as potential markers of oligodendrocytes, extracellular inflammation, gliosis, and vasogenic edema.<sup>43-45</sup> Thus, significant increases in extra-axonal diffusion have been previously reported in patients with mild cognitive impairment, Alzheimer disease, as well as MTBI, particularly in callosal regions.<sup>6,45</sup> The results of multivariate regression analysis, which assesses the impact of the relationships between multiple WM regions and IHSPT scores simultaneously, are consistent with the mediation analysis results showing significant associations of several callosal and noncallosal WM microstructures with IHSPT scores in the healthy control group but fewer regions in the MTBI group (Online Supplemental Data).

There are several limitations to this study. First, it includes a relatively small number of total subjects. The variability between patients in the early phases (<1 month postinjury) of MTBI results in a heterogeneous sample, which may dilute the generalizability of the results. The use of this method to inform the degree of injury in the context of clinical presentation and symptoms on an individual level would require larger cohorts. Second, the mediation model used in this study includes a single mediator, and there is a potential for multiple mediators that warrants further studies. Third, analyses were performed on MR images obtained from 2 scanners. We did reduce interscanner variability by using an established data-harmonization method, ComBat.<sup>38</sup>

which was performed on a larger-scale data set of 125 subjects, including diffusion images from other MTBI studies using the same diffusion sequence. Biologic variabilities such as age, sex, and disease group were preserved while removing interscanner variability. Fourth, although groups were not significantly different in terms of sex ( $P = .75$ , Fisher exact test), there may still be possible limitations in our analysis due to potential differences in terms of different interhemispheric connectivity between men and women.<sup>46</sup> This issue warrants further study with larger cohorts. Finally, a small percentage of individuals does have hemispheric codominance for language, making it difficult to accurately capture interhemispheric speed of processing using this tool. In most individuals, the left hemisphere is dominant for language; however, there is variability across the population. To reduce the confounding effects of handedness in IHSPT test performance, we excluded non-right-handed individuals.

## CONCLUSIONS

This study reveals significant WM mediators that affect the relationships between callosal microstructure and interhemispheric processing in healthy controls, supporting the idea that callosal interhemispheric communication is also influenced by neighboring WM microstructures. In MTBI, a loss of normal relationships is observed. This disruption may contribute to the subtle symptoms central to MTBI, especially those involving complex tasks. Future longitudinal studies with a larger cohort would provide insight into the temporal dynamics of interhemispheric recovery after MTBI.

## ACKNOWLEDGMENTS

This work was also performed under the rubric of the Center for Advanced Imaging Innovation and Research (CAI2R), a National Institute of Biomedical Imaging and Bioengineering Biomedical Technology Resource Center (National Institutes of Health, P41 EB017183).

Disclosure forms provided by the authors are available with the full text and PDF of this article at [www.ajnr.org](http://www.ajnr.org).

## REFERENCES

- Hiploylee C, Dufort PA, Davis HS, et al. **Longitudinal study of post-concussion syndrome: not everyone recovers.** *J Neurotrauma* 2017; 34:1511–23 [CrossRef Medline](#)
- Levin HS, Diaz-Arrastia RR. **Diagnosis, prognosis, and clinical management of mild traumatic brain injury.** *Lancet Neurol* 2015; 14:506–17 [CrossRef Medline](#)
- McAllister TW, Ford JC, Ji S, et al. **Maximum principal strain and strain rate associated with concussion diagnosis correlates with changes in corpus callosum white matter indices.** *Ann Biomed Eng* 2012;40:127–40 [CrossRef Medline](#)
- Patton DA, McIntosh AS, Kleiven S. **The biomechanical determinants of concussion: finite element simulations to investigate tissue-level predictors of injury during sporting impacts to the unprotected head.** *J Appl Biomech* 2015;31:264–68 [CrossRef Medline](#)
- Chung S, Fieremans E, Wang X, et al. **White matter tract integrity: an indicator of axonal pathology after mild traumatic brain injury.** *J Neurotrauma* 2018;35:1015–20 [CrossRef Medline](#)
- Chung S, Chen J, Li T, et al. **Investigating brain white matter in football players with and without concussion using a biophysical model from multi-shell diffusion MRI.** *AJNR Am J Neuroradiol* 2022;43:823–[CrossRef Medline](#)
- Rutgers DR, Fillard P, Paradot G, et al. **Diffusion tensor imaging characteristics of the corpus callosum in mild, moderate, and severe traumatic brain injury.** *AJNR Am J Neuroradiol* 2008; 29:1730–35 [CrossRef Medline](#)
- Aoki Y, Inokuchi R, Gunshin M, et al. **Diffusion tensor imaging studies of mild traumatic brain injury: a meta-analysis.** *J Neurol Neurosurg Psychiatry* 2012;83:870–76 [CrossRef Medline](#)
- Huynh-Le MP, Tibbs MD, Karunamuni R, et al. **Microstructural injury to corpus callosum and intrahemispheric white matter tracts correlate with attention and processing speed decline after brain radiation.** *Int J Radiat Oncol Biol Phys* 2021;110:337–47 [CrossRef Medline](#)
- Quigley M, Cordes D, Turski P, et al. **Role of the corpus callosum in functional connectivity.** *AJNR Am J Neuroradiol* 2003;24:208–12 [Medline](#)
- Marquez de la Plata CD, Garces J, Shokri Kojori E, et al. **Deficits in functional connectivity of hippocampal and frontal lobe circuits after traumatic axonal injury.** *Arch Neurol* 2011;68:74–84 [CrossRef Medline](#)
- Bai L, Bai G, Wang S, et al. **Strategic white matter injury associated with long-term information processing speed deficits in mild traumatic brain injury.** *Hum Brain Mapp* 2020;41:4431–41 [CrossRef Medline](#)
- Schulte T, Muller-Oehring EM. **Contribution of callosal connections to the interhemispheric integration of visuomotor and cognitive processes.** *Neuropsychol Rev* 2010;20:174–90 [CrossRef Medline](#)
- Bacon JH, Bacon T, Kister I, et al. **Posterior corpus callosum atrophy is correlated with worse performance on inter-hemispheric speed of processing task in unimpaired MS patients.** In: *Proceedings of the Annual Meeting of the American Academy of Neurology*, April 18–25, 2015. Washington, DC: No. 148
- Bloom JS, Hynd GW. **The role of the corpus callosum in interhemispheric transfer of information: excitation or inhibition?** *Neuropsychol Rev* 2005;15:59–71 [CrossRef Medline](#)
- Basser PJ, Mattiello J, LeBihan D. **Estimation of the effective self-diffusion tensor from the NMR spin echo.** *J Magn Reson B* 1994; 103:247–54 [CrossRef Medline](#)
- Jensen JH, Helpern JA, Ramani A, et al. **Diffusional kurtosis imaging: the quantification of non-gaussian water diffusion by means of magnetic resonance imaging.** *Magn Reson Med* 2005;53:1432–40 [CrossRef Medline](#)
- Novikov DS, Fieremans E, Jespersen SN, et al. **Quantifying brain microstructure with diffusion MRI: theory and parameter estimation.** *NMR Biomed* 2019;32:e3998 [CrossRef Medline](#)
- Coelho S, Baete SH, Lemberskiy G, et al. **Reproducibility of the standard model of diffusion in white matter on clinical MRI systems.** *Neuroimage* 2022;257:119290 [CrossRef Medline](#)
- Jelescu IO, Fieremans E. **Chapter 2 - Sensitivity and specificity of diffusion MRI to neuroinflammatory processes.** In: Cornelia Laule, John D. Port, ed. *Advances in Magnetic Resonance Technology and Applications*. Academic Press; 2023;9: 31–50
- Coronado-Leija R, Abdollahzadeh A, Lee HH, et al. **Volume electron microscopy in injured rat brain validates white matter microstructure metrics from diffusion MRI.** *ArXiv [Preprint]*. 2024 Jan 9; arXiv:2310.04608v2 [Medline](#)
- Liao Y, Coelho S, Chen J, et al. **Mapping brain microstructure in vivo in health and disease using diffusion MRI.** *ArXiv* 2023. <https://arxiv.org/abs/2307.16386>. Accessed January 31, 2024
- Jelescu IO, Zurek M, Winters KV, et al. **In vivo quantification of demyelination and recovery using compartment-specific diffusion MRI metrics validated by electron microscopy.** *Neuroimage* 2016;132:104–14 [CrossRef Medline](#)
- Jelescu IO, Veraart J, Adisetiyo V, et al. **One diffusion acquisition and different white matter models: how does microstructure change in human early development based on WMTI and NODDI?** *Neuroimage* 2015;107:242–56 [CrossRef Medline](#)
- Hui ES, Fieremans E, Jensen JH, et al. **Stroke assessment with diffusional kurtosis imaging.** *Stroke* 2012;43:2968–73 [CrossRef Medline](#)
- de Kouchkovsky I, Fieremans E, Fleysher L, et al. **Quantification of normal-appearing white matter tract integrity in multiple sclerosis: a diffusion kurtosis imaging study.** *J Neurol* 2016;263:1146–55 [CrossRef Medline](#)
- Chung S, Wang X, Fieremans E, et al. **Altered relationship between working memory and brain microstructure after mild traumatic brain injury.** *AJNR Am J Neuroradiol* 2019;40:1438–44 [CrossRef Medline](#)
- Kim A, Bacon J, Bacon T, et al. **Correlation of quantitative MR metrics of morphology and lesion load with performance on a novel inter-hemispheric speed of processing task in multiple sclerosis patients.** In: *Proceedings of the Annual Meeting of the American Society of Neuroradiology*. April 25–30, 2015. Chicago, Illinois
- Kay T, Harrington DE, Adams R, et al. **Definition of mild traumatic brain injury.** *J Head Trauma Rehabil* 1993;8:86–87
- Potter S, Leigh E, Wade D, et al. **The Rivermead Post Concussion Symptoms Questionnaire: a confirmatory factor analysis.** *J Neurol* 2006;253:1603–14 [CrossRef Medline](#)
- Setsompop K, Gagoski BA, Polimeni JR, et al. **Blipped-controlled aliasing in parallel imaging for simultaneous multislice echo planar imaging with reduced g-factor penalty.** *Magn Reson Med* 2012; 67:1210–24 [CrossRef Medline](#)
- Andersson JL, Skare S, Ashburner J. **How to correct susceptibility distortions in spin-echo echo-planar images: application to diffusion tensor imaging.** *Neuroimage* 2003;20:870–88 [CrossRef Medline](#)
- Veraart J, Novikov DS, Christiaens D, et al. **Denosing of diffusion MRI using random matrix theory.** *Neuroimage* 2016;142:394–406 [CrossRef Medline](#)
- Ades-Aron B, Veraart J, Kochunov P, et al. **Evaluation of the accuracy and precision of the diffusion parameter Estimation with Gibbs and NoisE removal pipeline.** *Neuroimage* 2018;183:532–43 [CrossRef Medline](#)
- Lee HH, Novikov DS, Fieremans E. **Removal of partial Fourier-induced Gibbs (RPG) ringing artifacts in MRI.** *Magn Reson Med* 2021;86:2733–50 [CrossRef Medline](#)
- Smith SM, Jenkinson M, Woolrich MW, et al. **Advances in functional and structural MR image analysis and implementation as FSL.** *Neuroimage* 2004;23(Suppl 1):S208–19 [CrossRef Medline](#)
- Standard Model Imaging (SMI) toolbox. <https://github.com/NYU-DiffusionMRI/SMI>. Accessed January 31, 2024
- Fortin JP, Parker D, Tunc B, et al. **Harmonization of multi-site diffusion tensor imaging data.** *Neuroimage* 2017;161:149–70 [CrossRef Medline](#)

39. Johnson WE, Li C, Rabinovic A. **Adjusting batch effects in microarray expression data using empirical Bayes methods.** *Biostatistics* 2007;8:118–27 [CrossRef Medline](#)
40. Mori S, Oishi K, Jiang H, et al. **Stereotaxic white matter atlas based on diffusion tensor imaging in an ICBM template.** *Neuroimage* 2008;40:570–82 [CrossRef Medline](#)
41. Preacher KJ, Hayes AF. **SPSS and SAS procedures for estimating indirect effects in simple mediation models.** *Behav Res Methods Instrum Comput* 2004;36:717–31 [CrossRef Medline](#)
42. Shenton ME, Hamoda HM, Schneiderman JS, et al. **A review of magnetic resonance imaging and diffusion tensor imaging findings in mild traumatic brain injury.** *Brain Imaging Behav* 2012;6:137–92 [CrossRef Medline](#)
43. Taquet M, Jankovski A, Rensonnet G, et al. **Extra-axonal restricted diffusion as an in-vivo marker of reactive microglia.** *Sci Rep* 2019;9:13874 [CrossRef Medline](#)
44. Grossman EJ, Kirov II, Gonen O, et al. **N-acetyl-aspartate levels correlate with intra-axonal compartment parameters from diffusion MRI.** *Neuroimage* 2015;118:334–43 [CrossRef Medline](#)
45. Fieremans E, Benitez A, Jensen JH, et al. **Novel white matter tract integrity metrics sensitive to Alzheimer disease progression.** *AJNR Am J Neuroradiol* 2013;34:2105–12 [CrossRef Medline](#)
46. Ingalhalikar M, Smith A, Parker D, et al. **Sex differences in the structural connectome of the human brain.** *Proc Natl Acad Sci U S A* 2014;111:823–28 [CrossRef Medline](#)